AIChE WILEY InterScience DISCOVER SOMETHING GREAT

FLUID MECHANICS AND TRANSPORT PHENOMENA

Polymer Flocculation of Calcite: Experimental Results from Turbulent Pipe Flow

Alex R. Heath
A. J. Parker Cooperative Research Centre for Hydrometallurgy (CSIRO Minerals), Clayton South, Victoria, Australia

Parisa A. Bahri
A. J. Parker Cooperative Research Centre for Hydrometallurgy (Murdoch University), School of Engineering-Rockingham Campus, Western Australia

Phillip D. Fawell and John B. Farrow
A. J. Parker Cooperative Research Centre for Hydrometallurgy (CSIRO Minerals), Waterford, Western Australia

DOI 10.1002/aic.10729
Published online December 5, 2005 in Wiley InterScience (www.interscience.wiley.com).

The kinetics of aggregation/breakage of calcite particles flocculated with a high-molecular-weight polymer flocculant has been studied in turbulent pipe flow. The mean flocculation residence time was varied by changing the length of pipe between the flocculant injection point and the in-stream particle-sizing probe (Lasentec FBRM). A variety of pipe sizes and flow rates were used to produce a range of mean fluid shear rates. The mean shear rate was calculated from the pressure drop along the pipe reactor, as measured by manometer, and was found to vary markedly as a function of both the solid fraction and aggregate size. Increased fluid shear increased the initial mixing and aggregation rates, but ultimately lead to a reduced final aggregate size due to increased aggregate breakage. Several other process variables were also studied, with the aggregate size increased with flocculant dosage and primary particle size, but reduced at higher solid fraction. © 2005 American Institute of Chemical Engineers *AIChE J,* 52: 1284–1293, 2006
Keywords: flocculation, particle/count/measurements, reaction kinetics

Introduction

Solid-liquid separation in mineral processing and wastewater treatment is frequently performed by gravity sedimentation.[1,2,3,4,5,6] Fine particles settle slowly in viscous flow, and coagulants or flocculants are frequently added to bond the fine particles into aggregates, increasing their settling rate. Prior to the addition of the coagulant or flocculant the particles are prevented from aggregating by a surface charge that causes electrostatic repulsion. However, this repulsion can be overcome by the addition of soluble ions (coagulants) that are attracted to the particle surface where they neutralize and compress the electrical double layer. The particles are then able to approach each other closely enough that van der Waals attractive forces can hold the particles together as stable aggregates.[7,8]

In mineral processing applications, high-molecular-weight ($\sim 20 \times 10^6$ g mol^{-1}) polymer flocculants have largely replaced simple coagulants, producing larger and denser aggregates, substantially increasing the solid-liquid separation performance.[9,10] Flocculants have polar or charged functional groups attached to a hydrocarbon backbone, making the polymer water-soluble and attracting it to the mineral surface. In addition to the effect of surface charge neutralization, high molecular weight flocculants are large enough to allow them to simultaneously coadsorb on two or more particles, forming a

Correspondence concerning this article should be addressed to A. R. Heath at alex.heath@csiro.au.

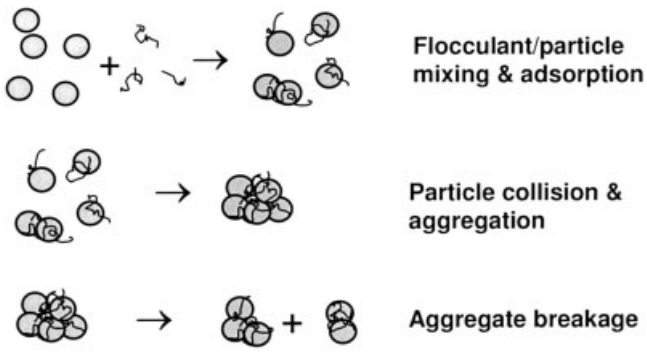

Figure 1. Stages (somewhat concurrent) of flocculation

polymer bridge that mechanically binds them together. This bridging process (Figure 1) is usually assumed to be the dominant bonding mechanism.[11,12] However, polymer flocculant molecules are somewhat fragile, and there is considerable evidence that aggregate breakage irreversibly reduces flocculant activity by chain scission or rearrangement. [9,11,13,14]

Experimental studies of aggregation kinetics are relatively difficult to perform, and may suffer a range of scale-up related problems.[3,15] Several laboratory-scale reactor designs have been used successfully, with a simple stirred and baffled tank being the most popular.[16] A stirred-tank reactor has the advantage of readily suspending solid particles at a comparatively low average shear rate.[3] The spatially averaged shear rate (G) is typically calculated from the mean energy dissipation rate[17-22]

$$G = \sqrt{\frac{\varepsilon}{\nu}} \tag{1}$$

where G = mean turbulent shear rate (s^{-1}); ε = energy dissipation rate per unit mass (J $s^{-1}kg^{-1}$ or m^2s^{-3}); ν = kinematic viscosity (m^2s^{-1}).

In a stirred tank the energy input can be estimated from the impeller power number,[16,21,23] or measured directly from the motor torque and rpm.[6,24] However, the shear rate will vary considerably through the tank, and is typically 5–10 times higher around the impeller.[21,25,26] Since both the aggregation and breakage rates are functions of the local shear rate, a simple volumetric average shear rate across the tank may not be an adequate description.[27]

In addition, a stirred-tank reactor is not suited to continuous flow for aggregation kinetics experiments, due to the broadening of the residence time distribution.[28] Restricting the laboratory vessel to a batch process leads to difficulties if aggregate sizing or settling rate measurements have to be taken *ex situ*. The action of removing the suspension of fragile aggregates (for example, by syringe or peristaltic pump) can alter the aggregate size.[2,29] Furthermore, if the required subsample is large, the volume remaining in the tank reactor may be significantly reduced, increasing the power dissipation rate per unit mass.

At the relatively high fluid shear (~10–1,000 s^{-1}) and solid fraction (~1–10% w/v) found in mineral processing thickener feedwells,[13,30] aggregation proceeds rapidly after flocculant/feed mixing/adsorption, with the short reaction time a further incentive to avoid time-consuming subsampling.

Another popular laboratory vessel for aggregation studies is a Couette device, where the suspension fills the gap between concentric rotating cylinders.[3,31,32,33,34] The laminar fluid shear rate can be calculated directly from the relative rotation speed, the cylinder radii, and the width of the gap.[35,36]

Aggregation studies have also been performed in pipe flow, either laminar,[37,38,39,40] or turbulent.[16,41,42,43] However, particles tend to settle out of laminar flow unless the pipe is vertical, or the particles neutrally buoyant. Turbulent pipe flow has the advantage of relatively homogeneous and isotropic turbulence in the core,[41] and the mean shear rate can be estimated from the pressure drop along the pipe[16,36,44,45] for example by manometer.

The aim of this study was to gather experimental aggregation/breakage kinetics data over a range of conditions (fluid shear rate, flocculant dosage, primary particle size and solid fraction) typical of a thickener/clarifier used in the mineral processing industry. These data has been used to develop a population balance model for the flocculation process that will be described in a subsequent article.

Particular attention is paid here to the effect of flocculation and the aggregate size on the suspension viscosity, which was calculated from pressure drop measurements along a turbulent pipe reactor.

Experimental

Aggregation/breakage kinetics were studied in turbulent pipe flow (Figure 2). A combination of pipe diameters (25.4 or 38.1 mm ID) and flow rates (14–40 L min^{-1}, 0.21–1.29 m s^{-1}) were used to produce a range of fluid shear rates. A series of flocculant injection nipples along the pipe produced a range of effective pipe lengths, and, hence, mean residence times assuming plug flow.

The pipe reactors were assembled from 1.83 m lengths of transparent acrylic pipe, with care taken to produce seamless joints and ensure a smooth inner pipe surface. Similarly, the flocculant injection nipples were attached to the outside of the pipe so that the inside surface of the pipe was only altered by drilled (2.4 mm) holes. The pipe was suspended approximately 1 m above the floor from a tensioned horizontal suspension cable arrangement (Figure 2), ensuring that the pipe reactor was kept straight and horizontal.

A focused beam reflectance measurement (FBRM) in-stream particle-sizing instrument (M500L, Lasentec) was placed in the flow at the end of the pipe reactor. The FBRM instrument has been described previously,[47] and was calibrated with the same solid substrate (calcite). In this case the coarse electronics option was used, giving the best measurement of aggregates that might otherwise be sized as a series of smaller particles.

The feed suspension was made up quantitatively in a 0.8 m^3 stirred/baffled feed tank, and the concentration confirmed gravimetrically by drying. A range of feed suspensions of different solid fraction (3.33 – 16.7% w/v, ϕ_{Exp} = 0.012-0.062, $\rho_{calcite}$ = 2710 kg m^{-3}) and/or mean primary particle size (2.36 – 24.3 μm) were used to simulate changes to the feed (Table 1). The various grades of calcite were sized independently by laser diffraction (Malvern MS 10 Mastersizer).

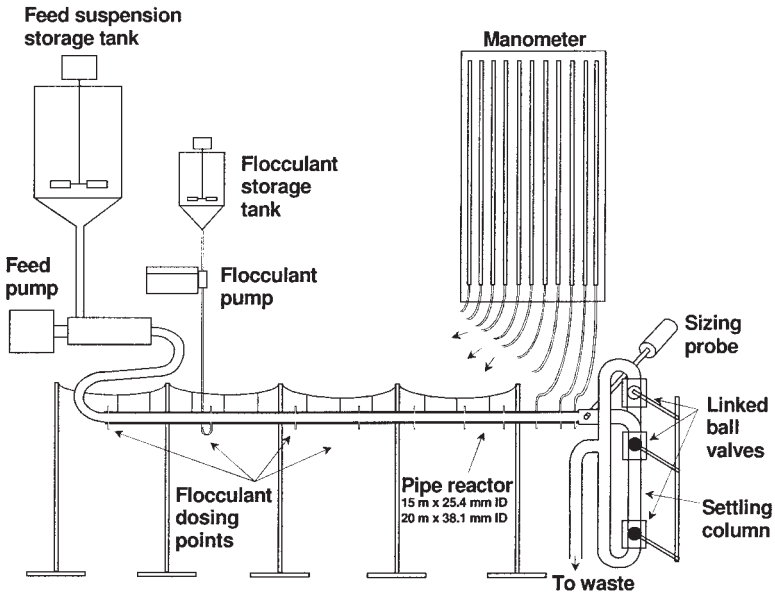

Figure 2. Laboratory equipment.

The feed suspension was delivered to the pipe reactor by a variable ratio drive positive displacement pump, and the flow rate confirmed by an on-line flow meter. A manometer bank (Figure 2) was used to measure the pressure drop along the pipe. The manometers were equilibrated from above, after flushing with water. This removed any solid from the manometer tubes, ensuring a known density (taken as 1,000 kg m^{-3}) and accurate pressure drop measurement.

Flocculant (ONDEO-Nalco 9902, 30% anionic acrylate/acrylamide copolymer with a nominal molecular weight of 15×10^6 g mol^{-1}) stock solution (0.02% w/v) was made up reproducibly (volume, stirrer speed and time) the day before use, minimizing any effect from flocculant aging.[48] The flocculant was dosed quantitatively on a mass (flocculant) for mass (solid) basis into the pipe reactor with a peristaltic pump, confirmed by a flow meter.

The addition of flocculant irreversibly alters the suspension, precluding the possibility of recycle. Consequently, after size and settling rate measurement the flocculated suspension was fed to a waste storage sump.

A matrix of experimental runs was performed according to Figure 3 and Table 1. The process variables of fluid shear, flocculant dosage, solid fraction and primary particle size were altered independently away from a common baseline point: 25.4 mm ID pipe, 14.01 L min^{-1} (mean velocity 0.461 m s^{-1}), 10% w/v (3.69% v/v) solid, volume-weighted average dia. 6.59 μm (by Malvern Mastersizer), and a flocculant dosage of 20 gt^{-1} (solid).

Aggregate size and settling rate measurements were made with flocculant injected at 13 positions (including a zero residence time — no flocculant) along the pipe, producing a range of residence times. The injection points were spaced according to a numerical progression, so that they were closer together at short residence times where the aggregate size increases rapidly.

This range of pipe lengths was used for each of the experi-

Table 1. Matrix of Pipe Reactor Experimental Runs (Bold Face Indicates Where Conditions Differ from Baseline)

Run No.	Pipe ID (m)	Flow Velocity (ms^{-1})	Solid ϕ (m^3 m^{-3}) [kg m^{-3}]	Mean d_p (μm)	Floc. Dose (g t^{-1})	Comment
1	0.0254	0.461	0.0369 [100]	6.59	20.0	Baseline run
2	0.0254	0.461	0.0369 [100]	6.59	**40.0**	Higher dosage
3	0.0254	0.461	0.0369 [100]	6.59	**10.0**	Lower dosage
4	0.0254	0.461	0.0369 [100]	6.59	**80.0**	Higher dosage
5	0.0254	0.461	0.0369 [100]	6.59	**5.0**	Lower dosage
6	0.0254	0.461	**0.0246 [66.7]**	6.59	20.0	Lower solid
7	0.0254	0.461	**0.0615 [167]**	6.59	20.0	Higher solid
8	0.0254	0.461	**0.0123 [33.3]**	6.59	20.0	Lower solid
9	0.0254	0.461	**0.0492 [133]**	6.59	20.0	Higher solid
10	0.0254	**0.781**	0.0369 [100]	6.59	20.0	Higher shear
11	0.0254	**1.294**	0.0369 [100]	6.59	20.0	Higher shear
12	**0.0381**	**0.554**	0.0369 [100]	6.59	20.0	Larger pipe
13	**0.0381**	**0.343**	0.0369 [100]	6.59	20.0	Lower shear
14	**0.0381**	**0.207**	0.0369 [100]	6.59	20.0	Lower shear
15	0.0254	0.461	0.0369 [100]	**15.08**	20.0	Larger particle
16	0.0254	0.461	0.0369 [100]	**2.36**	20.0	Smaller particle
17	0.0254	0.461	0.0369 [100]	**3.47**	20.0	Smaller particle
18	0.0254	0.461	0.0369 [100]	**24.26**	20.0	Larger particle

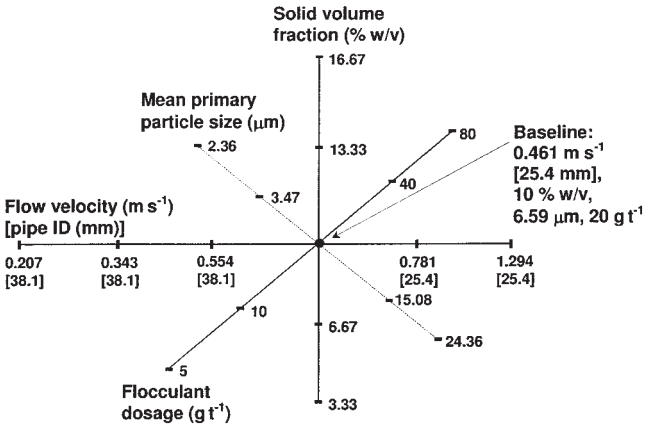

Figure 3. Experimental matrix.

mental conditions described by the sparse matrix described by Figure 3 and Table 1, giving a total of 13 × (6 + 4 + 4 + 4) data points.

Results and Discussion

Pressure drop to give viscosity and mean shear rate

The fluid shear rate (Eq. 1) is a critical variable in flocculation, affecting both the rate of aggregation and breakage, and was determined in this work using a manometer bank (Figure 2) to measure the pressure drop along the pipe reactor. Measuring the pressure drop allowed the calculation of the energy dissipation rate per unit mass of fluid (ε) from[21]

$$\varepsilon = \frac{V\Delta P}{\rho_f L} \tag{2}$$

where ε = energy dissipation rate per unit mass (J s^{-1} kg^{-1} or m^2 s^{-3}); V = mean flow velocity (m s^{-1}); ΔP = pressure drop along pipe (N m^{-2}); ρ_f = density of the fluid (kg m^{-3}); L = pipe length (m).

The energy dissipation rate will vary somewhat across the pipe but is reasonably homogeneous in the core of the flow, with the variation less than in a stirred tank.

The mean pipe flow velocity (V) is known experimentally via the volumetric flow rate and pipe ID, with the fluid density (ρ_f) calculated from the solid fraction and density

$$\rho_f = \rho_s\phi + \rho_w(1 - \phi) \tag{3}$$

where ρ_s = density of the solid (calcite = 2710 kg m^{-3}); ρ_w = density of water (taken as 1,000 kg m^{-3}); ϕ = solid volume fraction (m^3 m^{-3}).

The mean dissipation rate is readily calculated from Eq. 2, however, in order to calculate the mean fluid shear rate (Eq. 1), the suspension viscosity is also required. In most studies the viscosity is taken to be unchanged from pure water at the same temperature. This assumption is usually valid because most studies [23,34,49,50] have simulated conditions in water treatment clarifiers or river estuary system, which are characterized by a low solid fraction.[21,30]

However, feed streams to thickener units used in mineral processing have a considerably higher solid volume fraction, typically in the percent range,[21,30,52] leading to an increased fluid viscosity.[2] The volume of liquid enclosed within porous aggregates has the effect of further increasing the effective solid volume fraction and viscosity.[53] This effect is demonstrated experimentally (Figures 6, 8, 10 and 12) by an increased flow resistance and larger pressure drop along the pipe. In this case the use of positive displacement feed and flocculant pumps ensured constant flow rates, with the additional required energy readily supplied by the pumps since the overall back-pressure along the pipe was comparatively minor at ~1–10 × 10^3 N m^{-2} (0.01 – 0.1 atm).

Estimating the pressure drop through pipes is a common engineering problem, for example, when specifying pumps for pipelines. This has led to the development of the concept of a pipe Fanning friction factor (f), given by:[18,21,54,55]

$$f = \frac{D\Delta P}{2\rho V^2 L} = \frac{\varepsilon D}{2V^3} \tag{4}$$

where f = fanning friction factor (dimensionless); D = pipe diameter (m); ΔP = pressure drop along pipe (N m^{-2}); ρ = fluid density (kg m^{-3}); ε = energy dissipation rate (J s^{-1} kg^{-1} or m^2 s^{-3}); V = mean flow velocity (m s^{-1}) L = pipe length (m)

An alternative system is based on the Darcy friction factor,[56] differing only by a factor of 4.

Equation 4 is usually under-specified (ΔP or ε), and efforts have been made[54] to find alternative descriptions of the friction factor, usually as a function of the pipe Reynolds number (Re), with the equation by Blasius[57] being widely used

$$f = \frac{0.0791}{\mathrm{Re}^{1/4}} \tag{5}$$

$$\mathrm{Re} = \frac{DV\rho}{\mu} \tag{6}$$

Blasius' equation is correct for Newtonian flow in smooth pipes (as used here) for turbulent flow in the range 4,000 < Re < 100,000, however, a wide range of alternative equations have been proposed as a function of pipe roughness, Reynolds number, non-Newtonian behavior, and so on.[54]

Equations 5 and 6 were used to calculate the pressure drop along the pipe reactor with water only (no solid), allowing the estimation of the fluid viscosity (0.00105 N s m^{-3}, compared to the literature[56] value of 0.00102 N s m^{-3} at 20 °C), as shown by Figure 4. This served to confirm the equation, and that the dimensions had been converted correctly.

Equation 6 is tentatively assumed to hold for the turbulent flow of the aggregated suspensions, allowing the calculation of the suspension viscosity by combining Eqs. 4, 5 and 6

$$\mu = \frac{\Delta P^4 D^5}{(2 \times 0.0791)^4 \rho^3 V^7 L^4} \tag{7}$$

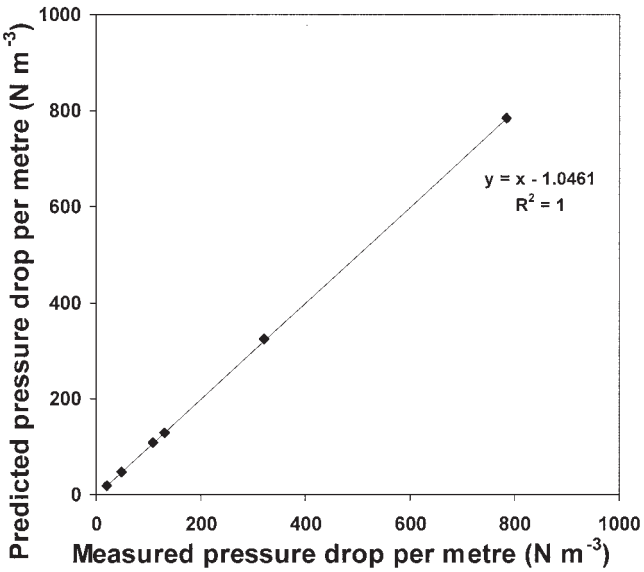

Figure 4. Measured and predicted (Eq. 7) pressure drop (per meter of pipe) of water under various flow regimes (as per Figure 3).

where μ = suspension viscosity (N s m^{-2}); D = pipe diameter (m); ΔP = pressure drop along pipe (N m^{-2}); ρ = fluid density (kg m^{-3}); V = mean flow velocity (m s^{-1}); L = pipe length (m).

The effect of flocculation increasing the suspension viscosity due to the formation of voluminous aggregates has been reported in the past for various systems, including polymer particles[58] and red blood cells.[59]

Solid particles are suspended by turbulent eddies, however, if the turbulence is insufficient for a given particle settling rate, the solid may stratify or even form a stationary bed on the bottom of the pipe reactor. This has the effect of throttling the flow and increasing the flow velocity and turbulence in the remaining clear portion of the pipe, preventing further settling. Eventually a steady-state condition is reached with a uniform stationary layer. The use of a transparent acrylic pipe allowed the observation of stratification/settling, aided by a fluorescent tube mounted behind the pipe to cast a shadow. Data collected when there was visible stratification/settling is of limited value, because the settled solid reduced the effective pipe diameter and decreased the average residence time.

Minimum suspension flow velocities in pipelines are usually described by the Durand[60] equation as a function of the mean flow velocity in the pipe and the particle size and density, although there is a variety of alternative relationships to choose from.[55,61,62,63,64,65,66,67]

Durand's equation is typically used for estimating the minimum transport velocity of relatively coarse particles (>1,000 μm) in full-scale pipelines, and has limited applicability to the current work with aggregated suspensions of fine particles. In the current case, stratification/settling was observed just above the transition to laminar flow (Re ~ 2,000–4,000).

The relatively high shear rate produced by small-scale turbulent pipe flow (~100–1,000 s^{-1} here) acts as an incentive to reduce the flow velocity and/or increase the pipe size. However, reducing the flow reduces the Reynolds number, causing the solid to settle out, while increasing the pipe size dramatically increases the required feed and disposal volumes (~5 tonnes calcite for the runs described here).

Alternatively, settling can be suppressed by substituting a smaller, or lower density, primary particle to reduce the settling rate. In this case a range of relatively fine primary particles were used (mean d_p = 2.36 – 24.3 μm). Using a lower density solid substrate (for example, latex) would have compromised the hindered settling rate measurements (to be described in a subsequent article), and may also have given a poor approximation of a mineral surface shape and chemistry.

Effect of mean fluid shear rate

Figure 5 shows the effect of changing the flow rate and pipe reactor inside diameter (ID) on the volume-weighted mean aggregate diameter. The flow rate and pipe ID were altered to produce a range of spatially-averaged shear rates (~100–1,000 s^{-1}, Table 1). A small pipe and high flow rate increases the flow resistance, the energy dissipation, and hence also increases the mean fluid shear rate. This initially leads to an increased aggregation rate due to faster flocculant/suspension mixing and particle collision, but ultimately leads to a reduced aggregate size due to an increased aggregate breakage rate. The reduction in final aggregate size at higher shear rates has been observed in other systems.[15,23,34,35,49,50,68,69]

The gentle reduction in the aggregate size at extended residence times observed here is typical behavior when polymer flocculants are used,[2,9,15,70,71] and is usually taken as evidence of flocculant deactivation by scission or rearrangement.[14,72,73,74] Conversely aggregates formed by coagulation with soluble salt normally reach a steady-state aggregate size, because in that case breakage is reversible.[23,34,49,50] The aggregate size reduction could also be due to aggregate compaction rather than aggregate breakage. However, a subsequent article also dealing with this calcite system will present settling rate data showing a decrease in settling velocity with the aggregate size. An increased aggregate density would be expected to increase the settling rate.

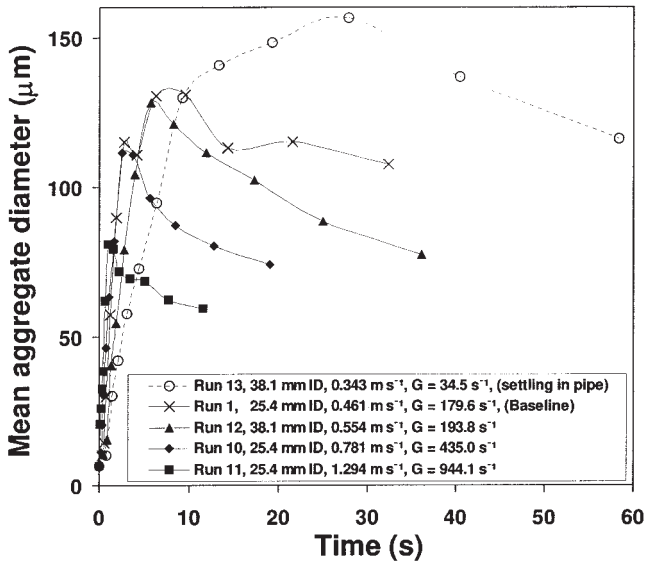

Figure 5. Effect of pipe size and fluid flow rate on volume-weighted mean aggregate size.

Flocculant dosage 20 g t^{-1}, d_p = 6.59 μm, 10% w/v solid.

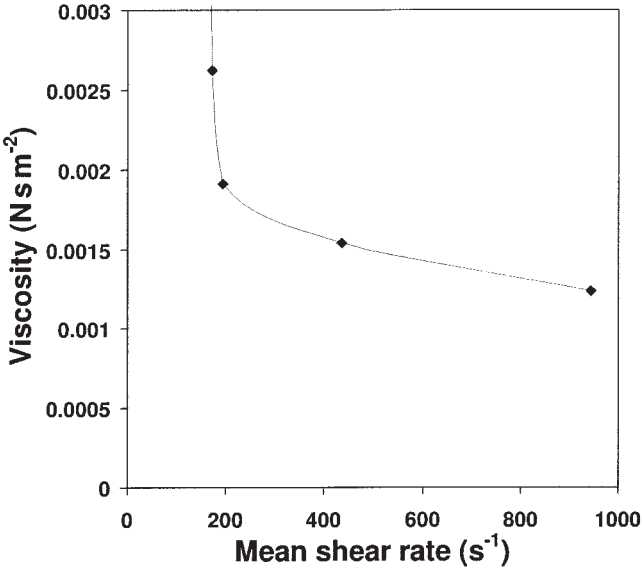

Figure 6. Aggregated suspension fluid viscosity estimated (Eq. 7) for the pressure drop along the pipe (see Figure 4 for aggregate size data).

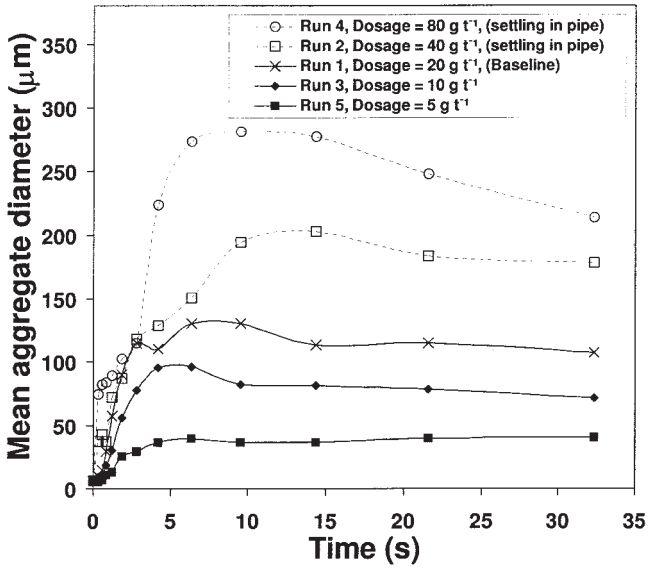

Figure 7. Effect of flocculant dosage on the volume-weighted mean aggregate size. 25.4 mm ID pipe, 0.461 m s^{-1}, d_p = 6.59 μm, 10% w/v solid.

Runs 1 and 13 shown in Figure 5 were an attempt to match the average shear rate in two different diameter pipes, using appropriate flow rates, respectively. The resulting mean aggregate size profiles through time are fairly similar, although the initial aggregation rate in the larger pipe (Run 13) is slower, perhaps due to the slower flocculant/suspension mixing. The larger pipe also produced a smaller aggregate size at extended residence times, although the difference appears too large to be explained entirely by the slightly higher shear rate. Other possible explanations include different flocculant/particle mixing, different hydrodynamic conditions (for example, shear profile across the pipe) or simply experimental variation.

Figure 6 shows the decrease in the average suspension viscosity flocculated at different shear rates, as calculated from the pressure drop using Eq. 7 (see also Table 1). The viscosity decreases at higher shear rates, because the decreased aggregate size (Figure 5) leads to a decreased aggregate porosity and, hence, effective solid fraction and suspension viscosity. The data is truncated to lower shear rates because stratification/settling in the pipe reactor throttled the flow, leading to a dramatically increased pressure drop.

Table 2 shows a summary of the results for viscosity, mean shear rate, friction factor, pipe Reynolds number etc for all of the experimental runs, as outlined in Figure 3 and Table 1, with the corresponding aggregate size data described in subsequent sections. In some cases the aggregated suspensions were observed to stratify/settle in the pipe reactor, leading to uncertainties in the solid fraction and average residence time, correspondingly shown in italics in Table 2, and these results should be interpreted with caution.

Table 2. Matrix of Pipe Reactor Experimental Results

Run No.	Viscosity (N s m^{-2})	Susp. Density (kg m^{-3})	Re	ε (m^2 s^{-3})	G (s^{-1})	f	Comment
1	0.0024	1063	5291	0.071	180	0.0093	Baseline run
2	*0.0165*	*1063*	*752*	*0.116*	*86*	0.0151	*Settling*
3	0.0016	1063	7681	0.065	207	0.0084	
4	*0.0509*	*1063*	*245*	*0.154*	57	0.0200	*Settling*
5	0.0014	1063	8759	0.063	217	0.0082	
6	0.0018	1042	6821	0.067	198	0.0087	
7	0.0030	1105	4294	0.075	166	0.0098	
8	0.0015	1021	8222	0.064	212	0.0083	
9	0.0027	1084	4637	0.074	171	0.0096	
10	0.0015	1063	13700	0.274	435	0.0073	
11	0.0012	1063	28173	1.039	944	0.0061	
12	0.0019	1063	11736	0.068	194	0.0076	
13	*0.0330*	*1063*	*421*	*0.037*	*34*	0.0174	*Settling*
14	*0.1675*	*1063*	*50*	*0.014*	*9*	0.0297	*Settling*
15	0.0058	1063	2158	0.089	128	0.0116	
16	0.0019	1063	6478	0.068	194	0.0088	
17	0.0016	1063	7996	0.064	210	0.0084	
18	*0.0101*	*1063*	*1237*	*0.103*	*104*	0.0133	*Settling*

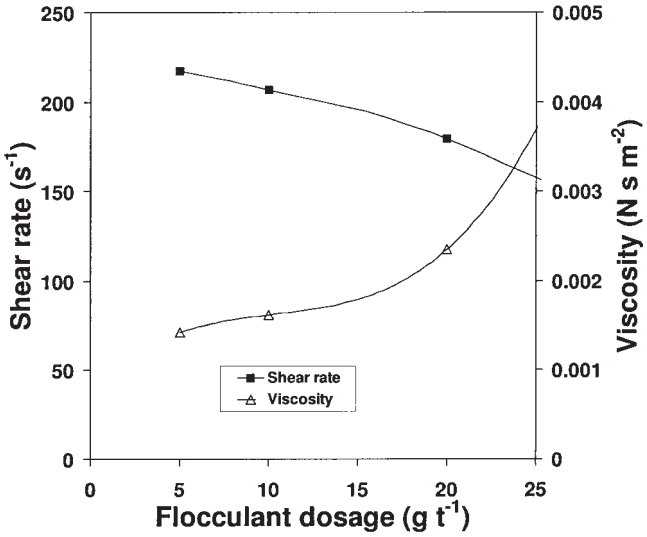

Figure 8. Effect of flocculant dosage on the measured fluid viscosity and shear rate.

Data is truncated due to settling in pipe reactor.

Effect of flocculant dosage

Figure 7 shows the increase in aggregate size with flocculant dosage. This can be attributed to either an increased capture efficiency (α = number of successful collisions/total number of collisions) and/or increased aggregate strength leading to a reduced breakage rate. Although the data show a faster initial aggregation rate at higher flocculant dosages, this must be at least partially attributed to increased initial flocculant/suspension mixing. The dilute (0.02%) flocculant stream was injected perpendicularly into the pipe reactor via a small hole in the pipe wall, causing a visible (clear acrylic pipe) increase in the turbulence around the injection point. The additional turbulence at the injection point increased with flocculant dosage, because the dosage was altered by changing the flocculant stream flow rate (rather than by increasing the flocculant stream concentration).

Flocculant/suspension macroscale mixing is likely to be highly scale dependent, and its importance is evidenced by the industrial practice of using a very dilute flocculant stream (0.01–0.1%[21,30]) and various proprietary feedwell designs to produce efficient mixing. It is difficult to replicate industrial-scale mixing conditions on a laboratory-scale, however, the use of emerging techniques like computational fluid dynamics,[75,76,77] or electrical impedance tomography[13,78,79,80,81] are likely to increase the understanding in this area.

While Figure 7 shows a regular increase in the aggregate size with flocculant dosage over the dosage range considered, there is some evidence to suggest[6,11,83] that very high flocculant dosages may lead to steric re-stabilization as the particle surface becomes overloaded with flocculant. However, it is unlikely that such a situation would occur in practice with modern high-molecular-weight flocculants, where adequate settling is achieved at dosages well below that required for full surface coverage. In addition, excessive flocculant addition may also reduce the unit's compression performance.[6,83]

Figure 8 shows the increase in viscosity and corresponding reduction in fluid shear as a function of the flocculant dosage. Again, this is attributed to the increased effective volume fraction enclosed by the aggregates as the aggregate size is increased. The possibility of the flocculant alone increasing the viscosity was discounted by performing an additional experiment under the same conditions, except without solid (water and flocculant only). Somewhat surprisingly, the pressure drop actually decreased fractionally (in the range 10 – 20% depending on the dosage — not shown). This phenomenon has been widely reported,[21,84,85,86] and is sometimes exploited to reduce the pumping costs in long pipelines.

Effect of primary particle size

Figure 9 shows the increase in aggregate size with primary particle size. This is likely to be caused by a combination of effects. As the primary particle size is increased, the total particle surface area per unit mass is decreased, leading to an increased flocculant surface coverage per area.[87] The increase in primary particle size will also increase the solid packing efficiency within the aggregate, decreasing the porosity, hence further increasing the aggregate strength.[9,88] The decreased porosity relative to aggregates of the same size, but containing smaller primary particles, tends to decrease the effective suspension solid fraction, subsequently tending to decrease the fluid viscosity, dissipation and breakage rates.

Overall however, the increased strength of aggregates formed from larger primary particles leads to a significantly increased aggregate size (and effective volume fraction occupied by the porous aggregates), a higher suspension viscosity (Figure 10) and dissipation rate. In this case the viscosity is the dominant term of Eq. 1, so the fluid shear is reduced with a larger primary particle (see Table 2).

Effect of suspension solid fraction

Figure 11 shows the reduction in aggregate size with increased solid fraction, a result that has been observed else-

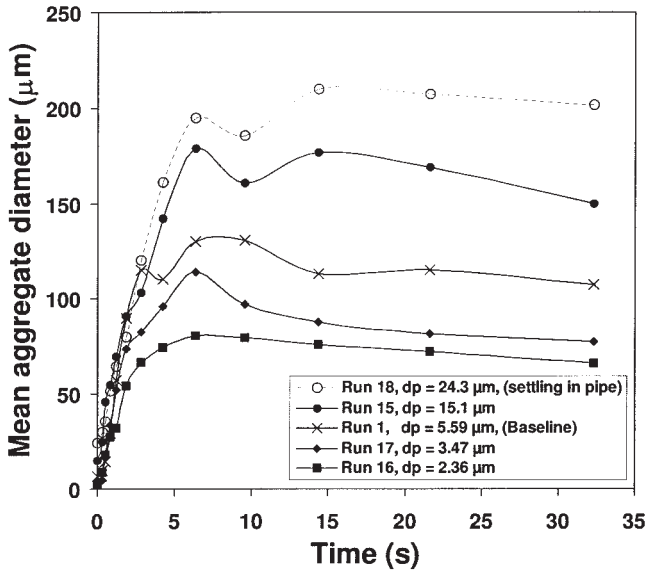

Figure 9. Effect of mean primary particle size on the volume-weighted mean aggregate size. 25.4 mm ID pipe, 0.461 m s^{-1}, flocculant dosage 20 g t^{-1}, 10% w/v solid.

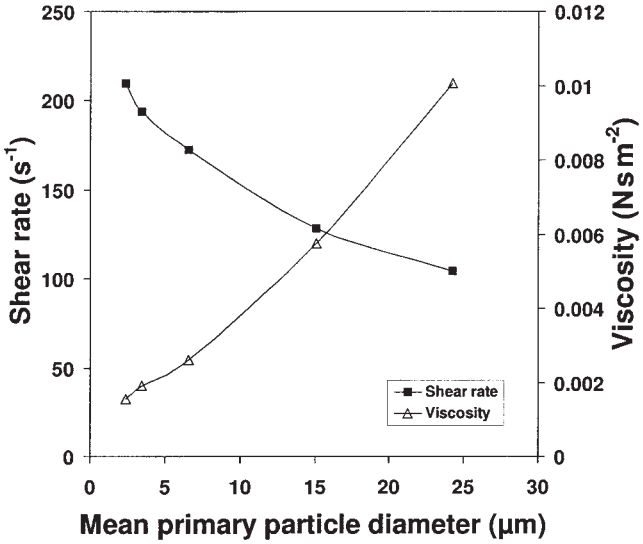

Figure 10. Effect of primary particle size on the measured fluid viscosity and shear rate of the aggregated suspensions.

The mean size is the volume-weighted mean as determined by laser diffraction (Malvern Mastersizer).

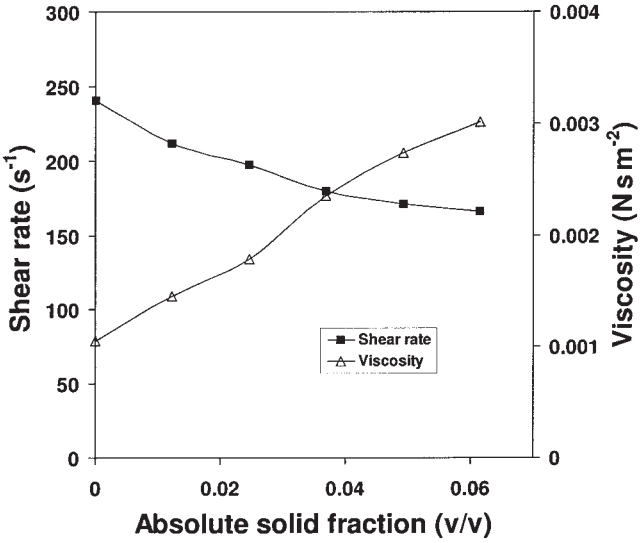

Figure 12. Effect of feed suspension solid fraction on the measured fluid viscosity.

where,[13,90] although not well understood. Figure 12 shows the increase in suspension viscosity and reduction in the shear rate as determined by manometer measurements. The reduction in the aggregate size at high solid fraction is attributed to a slightly reduced particle collision rate at lower shear, and an increased breakage rate due to the increase in viscosity and energy dissipation.

At very low solid fraction, there is evidence from other studies[44,90,91,93] to suggest that the aggregate size may be reduced, perhaps due to a decreased collision rate compared to the rate of aggregate breakage.

Collisional breakage is sometimes proposed to account for the reduction in size with solid fraction, that is, due to the increased collision rate at higher solids.[93,94] However, since aggregation is widely accepted to be second-order with respect to particle number, a simple breakage function also based on two-body collisions would also be second-order, with no net change in the aggregate size. Burban et al.[93] noted this and proposed a breakage mechanism, based on third-order kinetics and 3-body collisions, however, most workers continue to assume that breakage is caused mostly by fluid shear forces.

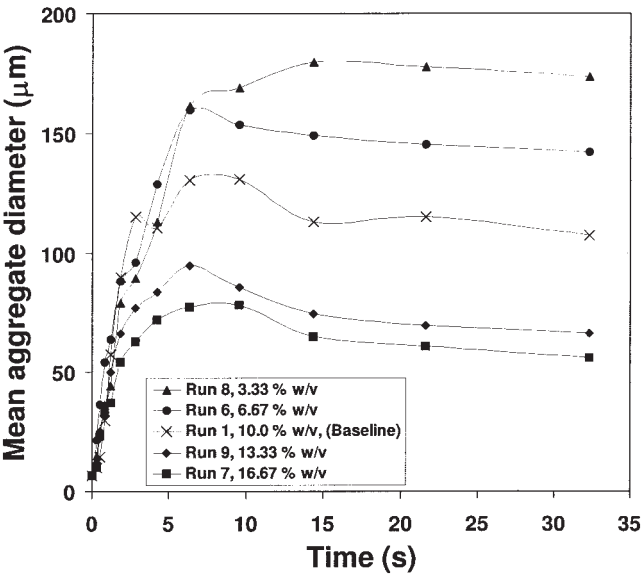

Figure 11. Effect of suspension solid fraction on the volume-weighted mean aggregate size. 25.4 mm ID pipe, 0.461 m s^{-1}, flocculant dosage 20 gt^{-1}, d_p = 6.59 μm.

Conclusions

The aggregation/breakage kinetics of calcite flocculation have been studied experimentally in turbulent pipe flow under a range of conditions, reflecting changes in likely industrial process variables: fluid shear, flocculant dosage, primary particle size, and solid volume fraction. Flocculation residence times were altered by varying the length of pipe between the flocculant injection point and the in-stream FBRM aggregate sizing probe. The pressure drop along the pipe was measured simultaneously by a manometer, allowing the calculation of the energy dissipation, fluid viscosity, and the mean shear rate as a function of the aggregate size.

Efforts were taken to match the conditions in the pipe reactor to those expected in a full-scale mineral processing plant, although scale-up remains an issue.

Flocculant/feed suspension mixing is faster with small volumes, and it is likely to be considerably overestimated by small-scale equipment. However, the major limitation is the tendency of solid to settle out of small-scale and low Reynolds number flows, restricting this study to a smaller primary particle size range and higher mean shear rates than are expected in practice. Despite these restrictions, the turbulent pipe reactor has given aggregation/breakage kinetic data for a concentrated mineral suspension under a range of well characterized, and reasonably representative conditions.

The aggregate size/time profiles obtained were characterized by an initial rapid increase in aggregate size over the first 2–6 s to a maximum size, after which there was a slower decline. The initial aggregation rate was found to increase at higher shear rates. However, the final aggregate size was ultimately limited by aggregate breakage, which is significantly increased at a higher shear rate. The aggregate size increased as a function of the flocculant dosage and primary particle size, but reduced at higher solid fraction.

Acknowledgments

This research has been supported by the Australian Government's Co-operative Research Centre (CRC) program, through the A.J. Parker CRC for Hydrometallurgy.

This work was conducted as part of the AMIRA P266 "Improving Thickener Technology" series of projects. The authors wish to thank the following companies for their support: Albian Sands Energy, Alcoa World Alumina, Anglo Gold, Anglo Platinum, Baker Process, Bateman Process Equipment, BHP Billiton, Cable Sands, Centaur Mining & Exploration, Ciba Specialty Chemicals, Cytec Australia Holdings, De Beers Consolidated Mines, EIMCO Process Equipment, Energy Resources Australia, GL&V/Dorr Oliver, Glencore AG, Hydro Aluminium AS, Iluka Resources Limited, Kumba Resources, Metso Minerals, Mt Isa Mines, Nabalco Pty, Ltd., ONDEO Nalco, Outokumpu Technology Pty, Pasminco, Pechiney Aluminium, Queensland Alumina Limited, Queensland Nickel (QNI), Rio Tinto, Tiwest, True North Energy, WMC Resources, Ltd., and Worsley Alumina Pty, Ltd.

Notation

D = pipe diameter, m
d = particle diameter, m
f = fanning friction factor, dimensionless
g = gravity, 9.8 m s^{-2}
L = pipe length, m
$\triangle P$ = pressure drop along pipe (N m^{-2}) given experimentally from: $\Delta P = \rho gh$
Re = pipe Reynolds number, dimensionless
V = mean flow velocity along pipe, m s^{-1}

Greek letters

ε = energy dissipation rate per unit mass, J $s^{-1}kg^{-1}$ or m^2s^{-3}
ρ_f = density of the fluid, kg m^{-3}
ρ_s = density of the solid, kg m^{-3}
ρ_w = density of water, kg m^{-3}
ϕ = solid volume fraction, [0,1]
μ = suspension viscosity, N s m^{-2}
ν = kinematic viscosity, m^2s^{-1}

Literature Cited

1. Amirtharajah A, Clark MM, Trussell RR. *Mixing in Coagulation and Flocculation.* USA: American Water Works Association Research Foundation; 1991.
2. Williams RA, ed. *Colloid and Surface Engineering, Applications in the Process Industries*, UK: Butterworth-Heinemann; 1992.
3. Shamlou PA. *Processing of Solid-Liquid Separations.* UK: Butterworth-Heinemann, Ltd., 1993.
4. Rushton A, Ward AS, Holdich RG. *Solid-Liquid Filtration and Separation Technology*. Germany: VCH; 1996.
5. Bustos MC, Concha F, Burger R, Tory EM. *Sedimentation and Thickening*. London: Kuwer Academic Publishers; 1999.
6. Svarovsky L, ed. *Solid-Liquid Separation*. 4th edition, Butterworth-Heinemann, UK. 2000.
7. Kohler HH. Thermodynamics of Adsorption from solution. In: Dobias B. *Coagulation and Flocculation: Theory and Applications*. New York: Marcel Dekker, 1993.
8. Hughes MA. Coagulation and Flocculation. In: Svarovsky L. *Solid-Liquid Separation*. 4th ed. UK: Butterworth-Heinemann; 2000.
9. Bagster DF, Aggregate behaviour in stirred vessels. In: Shamlou PA. *Processing of Solid-Liquid Separations.* UK: Butterworth-Heinemann, Ltd., 1993;26-58.
10. Farinato RS, Dubin PL. *Colloid-Polymer Interactions, From Fundamentals to Practice*. UK: John-Wiley & Sons; 1999.
11. Healy TW. Flocculation-dispersion behavior of quartz in the presence of a polyacrylamide flocculant. *J of Colloid Science*. 1961;16:609-617.
12. Gregory J. Fundamentals of flocculation. *CRC Critical Reviews in Environmental Control*. 1989;19:185-230.
13. Williams RA, Simons SJR. Handling colloidal materials. Chapter 2 in: Williams RA. *Colloid and Surface Engineering, Applications in the Process Industries*. UK: Butterworth-Heinemann; 1992.
14. Gregory J. Stability and flocculation of suspensions. In: Shamlou PA. *Processing of Solid-Liquid Separations.* UK: Butterworth-Heinemann, Ltd;1993:59-92.
15. Keys RO, Hogg R. Mixing problems in polymer flocculation. *Water 1978, AIChE Symposium Series*. 1978:63-72.
16. Ives KJ. Orthokinetic flocculation. In: Svarovsky, L. *Solid-Liquid Separation*, 4th ed. UK: Butterworth-Heinemann; 2000.
17. Cleasby JL. Is velocity gradient a valid turbulent flocculation parameter? *J Env Eng*. 1984;110:875-987.
18. Bird RB, Stewart WE, Lightfoot EN. *Transport Phenomena*. New York: John Wiley and Sons; 1960.
19. Davies JT. *Turbulence Phenomena*. London: Academic Press; 1972.
20. Clark MM. Critique of Camp and Stein's RMS velocity gradient. *J Env Eng*. 1985;111:741-754.
21. Perry HR, Green DW. *Perry's Chemical Engineers Handbook*. 7th ed., New York: McGraw-Hill; 1997.
22. Chen C-J, Jaw S-Y., *Fundamentals of Turbulence Modeling*, Washington, DC: Taylor & Francis; 1998.
23. Spicer PT, Pratsinis SE. Coagulation and fragmentation: Universal steady-state particle-size distribution. *AIChE J*. 1996;42:1612-1620.
24. Lu S, Ding Y, Guo J. Kinetics of fine particle aggregation in turbulence. *Advances in Colloid and Interface Sci*. 1998;78:197-235.
25. Koh PTL, Andrews JRG, Uhlerr PHT. Flocculation in stirred tanks. *Chem Eng Sci*. 1984;39:975-985.
26. Shamlou PA, Titchener-Hooker N. Aggregate behaviour in stirred vessels. In: Shamlou PA. *Processing of Solid-Liquid Separations.* UK: Butterworth-Heinemann, Ltd.; 1993.
27. Schuetz S, Piesche M. A model of the coagulation process with solid particles and flocs in a turbulent flow. *Chem Eng Sci.* 2002;57:4357-4368.
28. Nauman EB, Clark MM. Residence time distribution. In: Amirtharajah A et al. *Mixing in Coagulation and Flocculation*. Denver, CO: American Water Works Association Research Foundation; 1991:127-169.
29. Spicer PT, Pratsinis SE, Raper J, Amal R, Bushell G, Meesters G. Effect of shear schedule on particle size, density, and structure during flocculation in stirred tanks. *Powder Technol.* 1998;97:26-34.
30. Dahlstrom DA, Fitch EB. Thickening. Chapter 9.2 in: Weiss NL. *SME Mineral Processing Handbook*. New York: American Institute of Mining, Metallurgical, and Petroleum Engineers, Inc., Kingsport Press; 1985.
31. Fair GM, Gemmell RS. A mathematical model of coagulation. *J of Colloid Interface Sci*. 1964;19:360-372.
32. Ritchie R. *Certain Aspects of Flocculation as Applied to Sewage Purification*. London University; 1965. PhD Dissertation.
33. Akers RJ, Rushton, AG, Stenhouse JIT. Floc breakage: The dynamic response of the particle size distribution in a flocculated suspension to a step change in turbulent energy dissipation. *Chem Eng Sci*. 1987;42: 787-798.
34. Oles V. Shear-induced aggregation and breakup of polystyrene latex particles. *J of Colloid Interface Sci*. 1992;154:351-358.
35. Mühle K. Floc stability in laminar and turbulent flow. In: Dobias B. *Coagulation and Flocculation: Theory and Applications*. New York: Marcel Dekker; 1993;355-282.
36. Krutzer LLM, Van Diemen AJG, Stein HN. The influence of the type of flow on the orthokinetic coagulation rate. *J of Colloid Interface Sci*. 1995;171:429-438.
37. Gregory J. Flocculation in laminar flow tube. *Chem Eng Sci.* 1981;36: 1789-1794.
38. Eisenlauer J, Horn D. Influence of shear and salt on flocculation in laminar tube flow. in: Gregory J. *Solid-Liquid Separation.* Chichester: Ellis Horwood; 1984:183-195.
39. Whittington PN, George N. The use of laminar tube flow in the study

of hydrodynamic and chemical influences on polymer flocculation of escherichia coli. *Biotech. Bioeng.* 1992;40:451-458.
40. Suharyono H. and Hogg, R. Flocculation in flow through pipes and in-line mixers. *Minerals and Metallurgical Processing.* 1996;13:93-97.
41. Delichatsios MA, Probstein RF. Coagulation in turbulent flow: theory and experiment. *J of Colloid Interface Sci*. 1975; 51:394-405.
42. Klute R, Amirtharajah A. Particle destabilization and flocculation reactions in turbulent pipe flow. In: Amirtharajah A. et al. *Mixing in Coagulation and Flocculation*. Denver, CO: American Water Works Association Research Foundation; 1991:217-255.
43. Wigsten AL, Stratton RA. Polymer adsorption and particle flocculation in turbulent flow. *Polymer Adsorption and Dispersion Stability, ACS Symp. Ser. 240,* Goddard ED, Vincent B, eds. Am. Chem. Soc. 1984;429-444.
44. Thomas DG. Turbulent disruption of flocs in small particle size suspensions. *AIChE J*. 1964;10:517-523.
45. Matsuo T, Unno H. Forces acting on floc and strength of floc. *J. Envir. Eng. Div. ASCE*. 1981;107:527-545.
46. Gould BW. Velocity Shear Gradients in Pipes and Jets. *Effluent and Water Treatment J*. 1985;25:127-128.
47. Heath AR, Fawell PD, Bahri PA, Swift JD. Estimating average particle size by focussed beam reflectance measurement (FBRM). *Particle and Particle Systems Characterisation*. 2002;19:84-95.
48. Owen AT, Fawell PD, Swift JD, Farrow JB. The impact of polyacrylamide solution age on flocculation performance. *Intl J of Mineral Processing*. 2002;67:123-144.
49. Serra T, Casamitjana X. Effect of the shear and volume fraction on the aggregation and breakup of particles. *AIChE J*. 1998;44:1724-1730.
50. Flesch JC, Spicer PT, Pratsinis SE. Laminar and turbulent shear-induced flocculation of fractal aggregates. *AIChE J*. 1999;45:1114-1124.
51. Manning AJ, Dyer KR. A laboratory examination of the floc characteristics with regard to turbulent shearing. *Marine Geology*. 1999;60: 147-170.
52. Pearse MJ. *Gravity Thickening Theories: A Review* UK: Warren Spring Laboratory, Dept. of Industry, 1977.
53. Mills PDA, Goodwin JW, Grover BW. Shear field modification of strongly flocculated suspensions - aggregate morphology. *Colloid Polymer Sci*. 1991;269:949-963.
54. Govier, G.W. and Aziz, K. *The Flow of Complex Mixtures in Pipes.* Melbourne: Van Nostrand Reinhold Company; 1972.
55. Wasp EJ, Kenny JP, Gandhi RL. *Solid-Liquid Flow Slurry Pipeline Transportation*. Germany: Trans Tech Publications; 1977.
56. Daugherty RL, Franzini JB, Finnemore EJ. *Fluid Mechanics with Engineering Applications*. Singapore: McGraw-Hill; 1989.
57. Blasius H. Das Ähnlichkeitsgesetz bei Reibungsvorgängen in Flüssigkeiten. *Forschn. Gebiete Ingenierw*. 1913;No. 131.
58. Otsubo Y. Dilatant Flow of Flocculated Suspensions. *Langmuir*. 1992; 8:2336-2340.
59. Snabre P, Mills PI. Rheology of Weakly Flocculated Suspensions of Rigid Particles. *J de Physique III*. 1996;6:1811-1834.
60. Durand R. Basic relationships of the transportation of solids in pipes - Experimental research. Proceedings - *Minnesota International Hydraulics Convention.* 1953:89-103.
61. Spells KE. Correlations for use in transport of aqueous suspensions of fine solids through pipes. *Trans. Instn. Chem. Engrs*. 1955;33:80-84.
62. Zandi I, Govatos G. Heterogeneous flow of solids in pipelines. *Journal of the Hydraulics Division, Proceedings of the American Society of Civil Engineers*. May. 1967;145-159.
63. Kao TY, Wood PJ. *Trans. Soc. Min. Eng. of AIME*. 1974;255:39.
64. Turian RM, Yuan T-F. Flow of slurries in pipelines. *AIChE J*. 1977; 23:232-243.
65. Orokasar AR, Turian RM. The critical velocity in pipeline flow of slurries. *AIChE J*. 1980;26:550-558.
66. *Slurry Pumping Handbook*. Warman; 1989.
67. Shah SN, Lord DL. Critical velocity correlations for slurry transport with non-Newtonian fluids. *AIChE J*. 1991;37:683-870.
68. Curtis ASG, Hocking LM. Collision efficiency of equal spherical particles in a shear flow. *Trans Faraday Soc*. 1970;66:1381-1390.
69. Chin CJ, Yiacoumi S, Tsouris C. Shear-induced flocculation of colloidal particles in stirred tanks. *J of Colloid and Interface Sci*. 1998; 206:532-545.
70. Leu R, Ghosh MM. Polyelectrolyte characteristics and flocculation. *J. AWWA*. 1988;80:159-167.
71. Hogg R. Flocculation and dewatering. *Int. J. Miner. Process*. 2000; 58:223-236.
72. Sikora MD, Stratton RA. The shear stability of flocculated colloids. *Tappi*. 1981;64:97-101.
73. Stratton RA. Effect of agitation on polymer additives. *Tappi*. 1983; 66:141-144.
74. Ditter W, Eisenlauer J, Horn D. Laser optical methods for dynamic flocculation testing. In: Tadros *Effect of Polymers on Dispersion Processes*. London: Academic Press; 1982.
75. Lainé S, Phan L, Pellarin P, Robert P. Operating diagnostics on a flocculator-settling tank using fluent CFD software. *Wat Sci Tech*. 1999;39:155-162.
76. Ducoste JJ, Clark MM., Turbulence in flocculators: comparison of measurements and CFD simulations. *AIChE J*. 1999;45:432-436.
77. Farrow JB, Fawell PD, Johnston RRM et al., Recent developments in technologies and methodologies for improving thickener performance. *Chem Eng J*. 2000;80:149-155.
78. Brown BH, Barber DC, Saegar AD. Applied potential tomography: possible clinical applications. *Clin. Phy. Physiol. Meas*. 1985;6:109-121.
79. Webster JG. *Electrical Impedance Tomography*. Bristol: Adam Hilger; 1990.
80. Salkeld JA, Hunt A, Thorn R et al. Tomographic imaging of phase boundaries in multi-component processes. In: Williams RA, de Jaeger NC. *Advances in Measurement and Control of Colloidal Processes*. Oxford: Butterworth-Heinemann; 1991;95-106.
81. Dickin FJ, Hoyles BS, Hunt A et al., Tomographic imaging of industrial-process equipment - Techniques and applications. *IEE Proceedings-G Circuits Devices and Systems*. 1992;139:72-82.
82. Fleer GJ, Scheutjens JMHM. Modelling polymer adsorption, steric stabilization and flocculation. In: Dobias, B. *Coagulation and Flocculation: Theory and Applications*. New York: Marcel Dekker; 1993: 209-263.
83. Healy TW, Boger EV, White LR, Leong, YK, Scales PJ. Thickening and clarification; how much do we really know about dewatering? *AusIMM Extractive Metallurgy Conference*. Brisbane 3-6 July. 1994; 105-109.
84. Paterson RW, Abernathy FH. Turbulent flow drag reduction and degradation with dilute polymer solutions. *J of Fluid Mechanics*. 1970;43:689-710.
85. Moussa T, Tiu C. Factors affecting polymer degradation in turbulent pipe flow. *Chem Eng Sci*. 1994;49:1681-1692.
86. Rho T, Park J, Kim C, Yoon H-K, Suh H-S. Degradation of polyacrylamide in dilute solution. *Polym Degrad Stability*. 1996;51:287-293.
87. Hogg R., Polymer adsorption and flocculation. In: Laskowski JS. *Polymers in Mineral Processing*. Symposium organised by: The Canadian Institute of Mining, Metallurgy and Petroleum. Quebec, Canada August 1999, Met. Soc; 1993;3-17.
88. Dobias B. *Coagulation and Flocculation: Theory and Applications*. New York: Marcel Dekker; 1993.
89. Lick W, Lick J. Aggregation and disaggregation of fine-grained lake sediments. *J. Great Lakes Res.* 1988;14:514-523.
90. de Boer GBJ, Hoedemakers GFM, Thoenes D. Coagulation in turbulent flow: part I. *Chem Eng Res Des*. 1989;67:301-307.
91. de Boer GBJ, Hoedemakers GFM, Thoenes D. Coagulation in turbulent flow: part II. *Chem. Eng. Res. Des*. 1989;67:308-315.
92. Kobayashi M, Adachi Y, Ooi S. Breakup of fractal flocs in a turbulent flow. *Langmuir*. 1999;15:4351-4356.
93. Burban P, Lick W, Lick J. The flocculation of fine-grained sediments in estuarine waters. *J Geophys. Res*. 1989;94:8323-8330.
94. Ham RK, Christman RF. Agglomerate Size Changes in Coagulation. *J of the Sanitary Engineering Division. ASCE*. 1969;95:481-502.

Manuscript received May 30, 2005, and revision received Oct. 17, 2005.